

# Which observable offers better constraints on the optical potential?

M. Catacora-Rios,<sup>1,2</sup> G. B. King,<sup>1,2,3</sup> A. E. Lovell,<sup>4</sup> and F. M. Nunes<sup>1,2,\*</sup>

<sup>1</sup>*National Superconducting Cyclotron Laboratory, Michigan State University, East Lansing, MI 48824*

<sup>2</sup>*Department of Physics and Astronomy, Michigan State University, East Lansing, MI 48824-1321*

<sup>3</sup>*Department of Physics, Washington University, St. Louis, MO 63130, USA*

<sup>4</sup>*Theoretical Division, Los Alamos National Laboratory, Los Alamos, NM 87545*

(Dated: April 1, 2022)

**Background:** Modern statistical tools provide the ability to compare the information content of observables and provide a path to explore which experiments would be most useful to give insight into and constrain theoretical models.

**Purpose:** In this work we study these tools in the context of nuclear reactions with the goal of constraining the optical potential.

**Method:** We compare constraints coming from two sets of elastic data: angular distributions from unpolarized elastic scattering and vector analyzing powers. Three different statistical tools are examined: i) the sensitivity analysis based on derivatives; ii) the principle component analysis and iii) the Bayesian evidence. We apply these tools to study reactions on <sup>48</sup>Ca and <sup>208</sup>Pb each at two different beam energies.

**Results:** Considering the standard outputs of the Bayesian optimization, there is very little difference between the width of the posterior distributions and confidence intervals when only one of either differential cross sections or polarization data is used in the optimization. While the principle component analysis shows no significant difference between the two observables, the sensitivity studies indicate that the optical model parameters have larger variability with elastic scattering angular distribution data compared to the polarization data. The Bayesian evidence shows significant variability between the two observables, for several of the cases here considered.

**Conclusions:** Under the assumptions made in our study, our results show that, elastic scattering angular distributions have a larger impact in constraining the optical potentials than polarization data. In contrast, though, for most cases we studied, polarization data and elastic angular distributions contain similar information.

Keywords: uncertainty quantification, nucleon elastic scattering, transfer nuclear reactions, optical potential fitting

## I. INTRODUCTION

Nuclear reactions offer an incredibly versatile probe into nuclear structure, nuclear astrophysics, and nuclear applications beneficial to society and are particularly important in the context of rare isotopes [1]. One of the most important ingredients in predicting observables for nuclear reactions is the optical potential. The optical potential is an effective interaction between two composite nuclei that incorporates the complexity of the many-body problem into a multi-component multi-parameter complex form. The imaginary part of the optical potential accounts for all the processes that can take flux away from the incident elastic channel into other channels not included in the simplified model. In this work, we will focus on nucleon optical potentials, between either a proton or a neutron and a target nucleus ( $U_{NA}$ ). Because of its effective nature, the nucleon optical potential depends on the mass and charge of the target ( $A, Z$ ), and the energy of the beam ( $E_b$ ).

While there are many efforts to derive the optical potential starting from the NN interaction (e.g. [2–5]), for practical purposes, when computing reactions observables for  $A > 20$ , phenomenological optical potentials are typically used [6–8]. These are obtained from fitting

primarily elastic-scattering data, although other observables such as analyzing powers and total cross sections are sometimes also included in the fitting protocol.

Over the last few years, there has been substantial progress on quantifying uncertainties in nuclear reactions [9–11]. We have implemented and applied the Bayesian Markov Chain Monte Carlo method (MCMC) to a variety of reactions and concluded that when using elastic-scattering data at the appropriate energy with a typical 10% error, the resulting uncertainties in the observables are undesirably large (often larger than 50%), a consequence of degeneracies in the parameter space. In a recent work [11], we looked into ways to reduce the uncertainty by diversifying the data sets or by choosing data with optimum information content. Namely we investigated which parts of the angular distribution matter for constraining the cross sections, and whether data at nearby energies adds further restrictions on the parameters. We have also investigated the possibility of including polarization data through  $iT_{11}$ . To diagnose whether including different sets of data mattered, we compared directly the widths of the 95% confidence intervals. However comparing directly two confidence intervals obtained from constraints using two different sets of data has serious ambiguities: what is the appropriate confidence level to make this comparison? and at what angle should the conclusion be drawn? Ultimately we would like to be able to establish without ambiguity which data set (or sets) contain maximum information, resulting in minimum un-

---

\*Electronic address: nunes@nscl.msu.edu

certainty. For that, we turn to a wider set of diagnostic tools.

Borrowing from statistical methods applied in many other fields, in this work we inspect three different approaches: i) a sensitivity analysis based on derivatives of the observables with respect to the optical potential parameters, ii) the principal component analysis that can help to identify whether there is a combination of observables that can simplify the problem and iii) the Bayesian evidence that integrates the likelihood over the model space to quantify the information content of a given observable.

These statistical methods are not new; they have been widely applied to other fields and in the last few years have been ported into the nuclear domain. Sensitivity studies continue to provide insight into which parameters have the largest impact on the observables considered (see [12–14] for recent applications to nuclear structure). Principle component analyses, coming from the diagonalization of the sensitivity matrix, identify the best combinations of parameters or observables that should be considered to reduce the dimensionality of the model space. It is often used to construct emulators (e.g. [15–17]). Finally, the Bayesian factor, the ratio of the evidence associated with two models, provides an implementation of Occam’s razor: the simplest theory compatible with data should be used [18]. It is also used to discriminate between the information content of different data. This latter is the use made in the present work. Although calculating the Bayesian evidence is numerically challenging, there are already examples of applications to effective field theory [19] and to nuclear structure [14].

In this work, we performed calculations for elastic scattering of protons on  $^{48}\text{Ca}$  at 12 MeV and 21 MeV, neutrons on  $^{48}\text{Ca}$  at 12 MeV; protons on  $^{208}\text{Pb}$  at 30 and 61 MeV and neutrons on  $^{208}\text{Pb}$  at 30 MeV, to investigate which types of data are best suited to constrain the nucleon optical potential in this energy range. In section II we provide a brief description of the statistical tools to be used. This is followed by a detailed discussion of the results in Section III. Finally conclusions are drawn in Section IV.

## II. STATISTICAL METHODS

In this section, we briefly describe three diagnostic tools to quantify the information content of a given set of scattering data.

### A. Principle Component Analysis

The optical potential imprints itself on many reaction observables. As such we can consider a principle component analysis (PCA) on observable space. Parameter space is randomly sampled  $N$  times, generating a parameter set  $x_i$  for each run used to calculate a set of

observables  $y_i$ . The parameters and observable data is standardized (*i.e.*, mean-centered with a standard deviation of 1). We denote the standardized parameters and observables as  $\bar{x}$  and  $\bar{y}$ , respectively. The observable covariance matrix,  $\mathbf{C}$ , is then calculated as:

$$\mathbf{C}_{ab} = \frac{1}{N-1} \bar{y}_a^T \bar{y}_b. \quad (1)$$

The principal components of observable space ( $e_b$ ) are the eigenvectors of  $\mathbf{C}$ . The eigenvalues  $\lambda_b$  corresponding to the eigenvectors  $e_b$  can be used to organize the principal components. A larger value of  $\lambda_b$  means that a larger percentage of the variance in the data is captured by the corresponding  $e_b$ . To visualize the composition of the eigenvectors,  $e_b$ , we construct the weight matrix,

$$\mathbf{W}_{ab} = |\hat{y}_a \cdot e_b|, \quad (2)$$

where  $\hat{y}_a$  is the  $a^{\text{th}}$  unit vector in the observable space basis. Each column in  $\mathbf{W}$  is normalized to unity:

$$\sqrt{\sum_i \mathbf{W}_{ij}^2} = 1 \quad (3)$$

We can then assign a weight,  $w_a$ , to an observable,  $y_a$ :

$$w_a = \sum_b \lambda_b |\mathbf{W}_{ab}|. \quad (4)$$

This weight serves as a measure of the importance of the observable across the various principal components and it is often used to identify the most impactful observables.

### B. Sensitivity study with derivatives

Looking at the impact of variations of the observables on the parameters can help determine which optical model parameters are most sensitive to changes in specific observables, and therefore which observables are most important for constraining the optical model. A simple approach is to consider directly the covariance  $\tilde{\mathbf{C}}_{ia}$  of an observable  $\bar{y}_a$  and a parameter  $\bar{x}_i$ :

$$\mathbf{C}_{ia} = \frac{1}{N-1} \bar{x}_i^T \bar{y}_a. \quad (5)$$

We note that  $\mathbf{C}_{ia}$  relates to the observable covariance matrix through [16]:

$$\tilde{\mathbf{C}}_{ia} = \sum_b \left\langle \frac{\partial \bar{x}_i}{\partial \bar{y}_b} \right\rangle \mathbf{C}_{ba} \quad (6)$$

This relation can be inverted to provide the sensitivity:

$$\left\langle \frac{\partial \bar{x}_i}{\partial \bar{y}_a} \right\rangle = \tilde{\mathbf{C}}_{ib} \mathbf{C}_{ba}^{-1} \quad (7)$$

which quantifies the variation in parameter  $x_i$  caused by a variation in the observable  $y_a$ .

### C. Bayesian evidence

As opposed to the frequentist tools based on covariance matrices, Bayesian statistics is based on probability distributions. For some hypothesis,  $H$ , data,  $d$  and model,  $\mathcal{M}$ , Bayes' theorem is expressed as:

$$p(H|d, \mathcal{M}) = \frac{p(d|H, \mathcal{M})p(H|\mathcal{M})}{p(d|\mathcal{M})}, \quad (8)$$

which states that the posterior probability for the hypothesis,  $p(H|d, \mathcal{M})$ , taking the data and some assumptions about the model into account, is equal to the likelihood function,  $p(d|H, \mathcal{M})$  (the sampling distribution of the data assuming the hypothesis is correct), times the prior probability,  $p(H|\mathcal{M})$  (the physical knowledge of the model without any external information) divided by the Bayesian evidence  $p(d|\mathcal{M})$ .

While in previous works we have focused on evaluating the posterior distributions of parameters and subsequent confidence intervals of observables, in this work, we focus on the Bayesian evidence. This normalization factor provides a quantification of the information content of a given set of data. For a given model  $\mathcal{M}$  with a certain number of parameters  $\alpha$ , the Bayesian evidence is the integral of the likelihood function times the prior distribution over the entire parameter space:

$$p(d|\mathcal{M}) = \int_{\Omega_{\mathcal{M}}} p(d|\alpha, \mathcal{M})p(\alpha|\mathcal{M})d\alpha_{\mathcal{M}}. \quad (9)$$

The explicit calculation of this integral is difficult and computationally demanding as it involves multidimensional integration over all parameters. While the likelihood function might be sharply peaked within the prior range, long tails in the distributions can provide significant contributions to the integral.

In some applications, the Bayesian evidence integral is approximated analytically (e.g. [19]). This approximation is valid when the likelihood function is unimodal and the corresponding parameters are Gaussian. However, in our case, these conditions are not met (see Section III.B). Therefore, to obtain the Bayesian evidence for the optical model, we use the Monte-Carlo approximation to sample full space [20]. Then the integral in Eq. (9) becomes:

$$p(d|\mathcal{M}) = \frac{1}{N} \sum_{\alpha_i=1}^N p(d|\alpha_i, \mathcal{M}) \quad (10)$$

where  $N$  number of sampled parameter sets,  $\alpha_i$ , are drawn randomly from the prior distribution.

## III. RESULTS

We have studied a number of different elastic-scattering processes:  $^{48}\text{Ca}(n,n)$  at 12 MeV;  $^{48}\text{Ca}(p,p)$  at 12 MeV and 21 MeV;  $^{208}\text{Pb}(n,n)$  at 30 MeV;  $^{208}\text{Pb}(p,p)$

at 30 MeV and 61 MeV. A selection of these are shown in this section to illustrate the benefits and limitations of these various diagnostic tools.

All data used in this work is mock data, generated from the global optical potential [8] including a 10% error, similarly to what was done in [11]. For the polarization data, we introduced a lower limit for the error, determined by 5% of the maximum  $iT_{11}$  value. We initialized the optical potential parameters using the global optical model [6], and use wide Gaussian priors as in previous work [11] to ensure that the process is data driven. We considered only six free parameters for the optical potential, namely the depth, radius and diffuseness of a Woods-Saxon real term ( $V, r, a$ ) and the depth, radius and diffuseness of a surface imaginary term ( $W_s, r_s, a_s$ ). The remaining parameters were kept fixed as in [8]. Finally, we use the suite of codes QUILT-R [21] (more details on the MCMC calculations can be found in [9]).

### A. Confidence intervals resulting from the fit

We begin by analyzing the results for the 95% confidence intervals. In Fig. 1, we show the elastic angular distributions (top) and the polarization distributions (bottom) obtained when either the elastic angular distribution data is used (dark red interval) or the polarization data is used (light blue interval). Figs. 1(a) and (c) correspond to  $^{48}\text{Ca}(p,p)$  at 12 MeV while Figs. 1(b) and (d) correspond to  $^{48}\text{Ca}(p,p)$  at 21 MeV. Expectedly, confidence intervals are narrower for the elastic angular distribution when elastic angular distribution data is used. The same principle is true when polarization data is used: confidence intervals are narrower for  $iT_{11}$ .

However, these results alone do not provide sufficient basis to make a choice on which data set contains more information and provide a better constraint on the optical model.

### B. Posterior distributions

Next, we inspect the parameter posterior distributions. Table I contains the means and standard deviations for the six posterior distributions obtained in the cases under consideration, namely  $^{48}\text{Ca}(p,p)$  at 12 MeV and 21 MeV using either  $\frac{d\sigma}{d\Omega}$  or  $iT_{11}$  data in the optimization procedure. For completeness, the full posterior distributions for each of the six parameters are shown in the panels a-f of Fig. 2 and Fig. 3, together with the resulting  $\chi^2$  and likelihood distributions (panels g and h). The results using  $\frac{d\sigma}{d\Omega}$  data are shown in red (dark) and the results using  $iT_{11}$  data are shown in blue (light).

The red and blue distributions in Fig. 2 and Fig. 3 are mostly overlapping, indicating that the angular distributions and the polarization data lead to very similar minima in parameter space. Some posteriors present a semi-bimodal structure or extended tails. This is reflected in

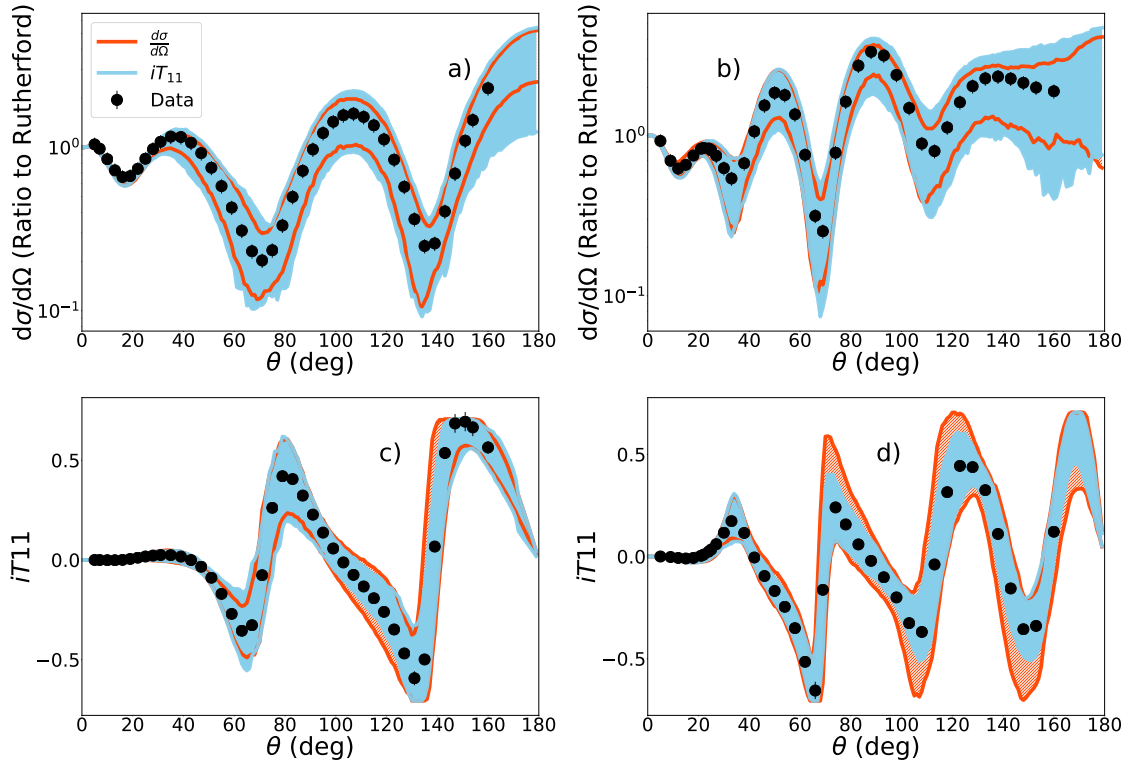


FIG. 1: 95% confidence intervals calculated using  $\frac{d\sigma}{d\Omega}$  data (red bands) or  $iT_{11}$  data (blue bands) in the optimization procedure: a)  $d\sigma/d\Omega$  for  $^{48}\text{Ca}(p,p)$  at 12 MeV; b)  $d\sigma/d\Omega$  for  $^{48}\text{Ca}(p,p)$  at 21 MeV; c)  $iT_{11}$  for  $^{48}\text{Ca}(p,p)$  at 12 MeV; d)  $iT_{11}$  for  $^{48}\text{Ca}(p,p)$  at 21 MeV.

Observable	E (MeV)	V (MeV)	r (fm)	a (fm)	$W_s$ (MeV)	$r_s$ (fm)	$a_s$ (fm)
$\frac{d\sigma}{d\Omega}$	12.0	59.48 (4.12)	1.173 (0.052)	0.699 (0.051)	9.476 (0.960)	1.294 (0.084)	0.571 (0.049)
$iT_{11}$	12.0	60.65 (5.22)	1.159 (0.057)	0.699 (0.067)	9.704 (0.954)	1.273 (0.079)	0.595 (0.080)
$\frac{d\sigma}{d\Omega}$	21.0	55.57 (4.11)	1.178 (0.052)	0.661 (0.057)	7.857 (0.767)	1.297 (0.083)	0.572 (0.051)
$iT_{11}$	21.0	57.16 (4.44)	1.165 (0.047)	0.691 (0.046)	8.011 (1.007)	1.260 (0.073)	0.579 (0.076)

TABLE I: Characteristics of the posteriors for the two  $^{48}\text{Ca}(p,p)$  elastic observables considered; the second column is the beam energy; the next three columns provide the means (standard deviations) for the depth, radius and diffuseness of the real part of the optical potential; the last three columns provide the means (standard deviations) for the depth, radius and diffuseness of the imaginary surface terms of the optical potential.

slight differences in the means and standard deviations shown in Table I, although the differences in the means are accounted for within the listed standard deviations. Even though at the peak, it may appear that some posteriors are narrow, one should note the long tails, which can result in a larger than expected standard deviation. Ultimately both sets of data lead to an identical likelihood function and therefore similar goodness of fit.

### C. Sensitivity study with derivatives

As shown in Sections III A and III B, when cross section data is compared with polarization data using the

basic Bayesian analysis tools, namely confidence intervals and posterior distributions, this leads to a draw. It is not possible to clearly identify which set of data contains more information to constrain the optical model. Both describe the data very well but give rise to rather large uncertainties. Keeping this motivation in mind, we now turn to other statistical tools.

A sensitivity study was performed to understand which observables lead to the largest variation in the parameters. The sets of parameters are drawn randomly from the posterior distributions of Section III A. The covariance matrices are then computed as described in Section II.

The average,  $\langle \frac{d\bar{x}_i}{d\bar{y}_a} \rangle$ , is obtained for either the elastic

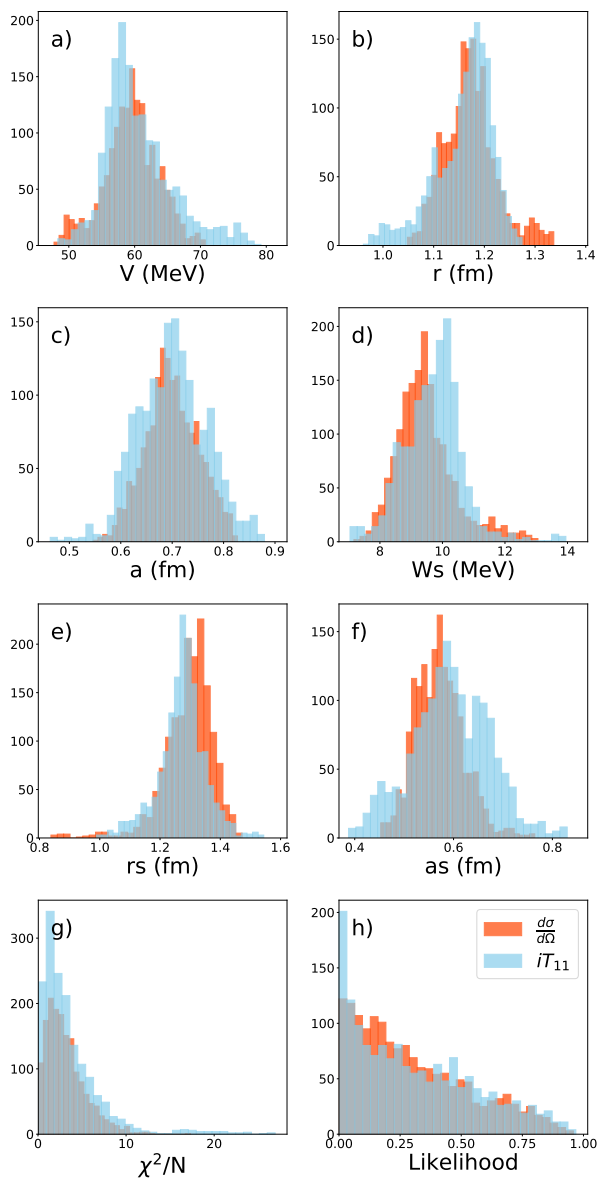


FIG. 2: Posterior distributions for the optical potential parameters (panels a-f) obtained for  $^{48}\text{Ca}(p,p)$  at 12 MeV:  $\frac{d\sigma}{d\Omega}$  data (dark red) and  $iT_{11}$  data (light blue);  $\chi^2$  and likelihood function (panels g and h, respectively).

angular distributions for angles in the range  $\theta = 20-165^\circ$  in intervals of  $5^\circ$ , or for the corresponding polarization observables. These are shown in Fig. 4 for  $^{48}\text{Ca}(n,n)$  at 12 MeV (panel a);  $^{48}\text{Ca}(p,p)$  at 12 MeV (panel b) and  $^{48}\text{Ca}(p,p)$  at 21 MeV (panel c). Based on these findings, we may opt to choose the elastic angular distribution over the polarization data to constrain the optical potential.

In previous work, we had identified that the angular distribution at different angles were strongly correlated [22]. By analyzing the sensitivities, we see that some angles appear to impact the parameters more than others. Most importantly, for the lowest energies the elastic

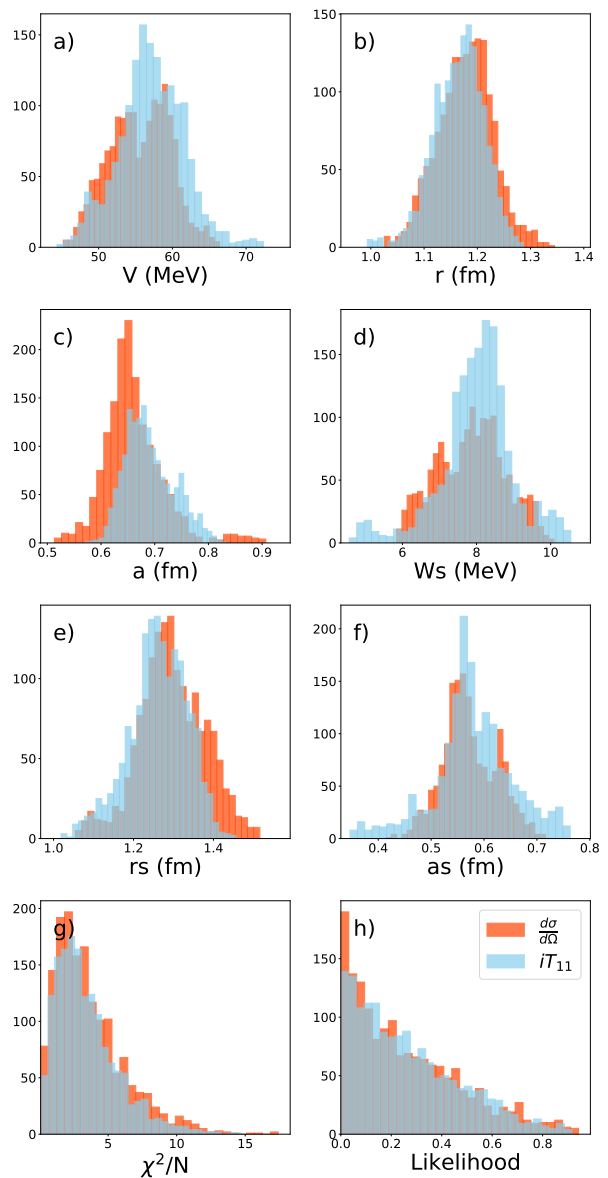


FIG. 3: Posterior distributions for the optical potential parameters (panels a-f) obtained for  $^{48}\text{Ca}(p,p)$  at 21 MeV:  $\frac{d\sigma}{d\Omega}$  data (dark red) and  $iT_{11}$  data (light blue);  $\chi^2$  and likelihood function (panels g and h, respectively).

cross section impacts mostly the surface imaginary depth and diffuseness while at the higher energy it impacts the real volume term too. This feature is understood given that at the lower energy the reaction is mostly peripheral [23]. The sensitivity plots suggest that elastic-scattering data can impact the parameters of the optical potential here considered more than the polarization data. We find a stronger sensitivity for the parameters involving spin-orbit force when considering the polarization data (not shown here). This confirms the general knowledge in the field [23].

Although we do not include figures on the Pb reactions,

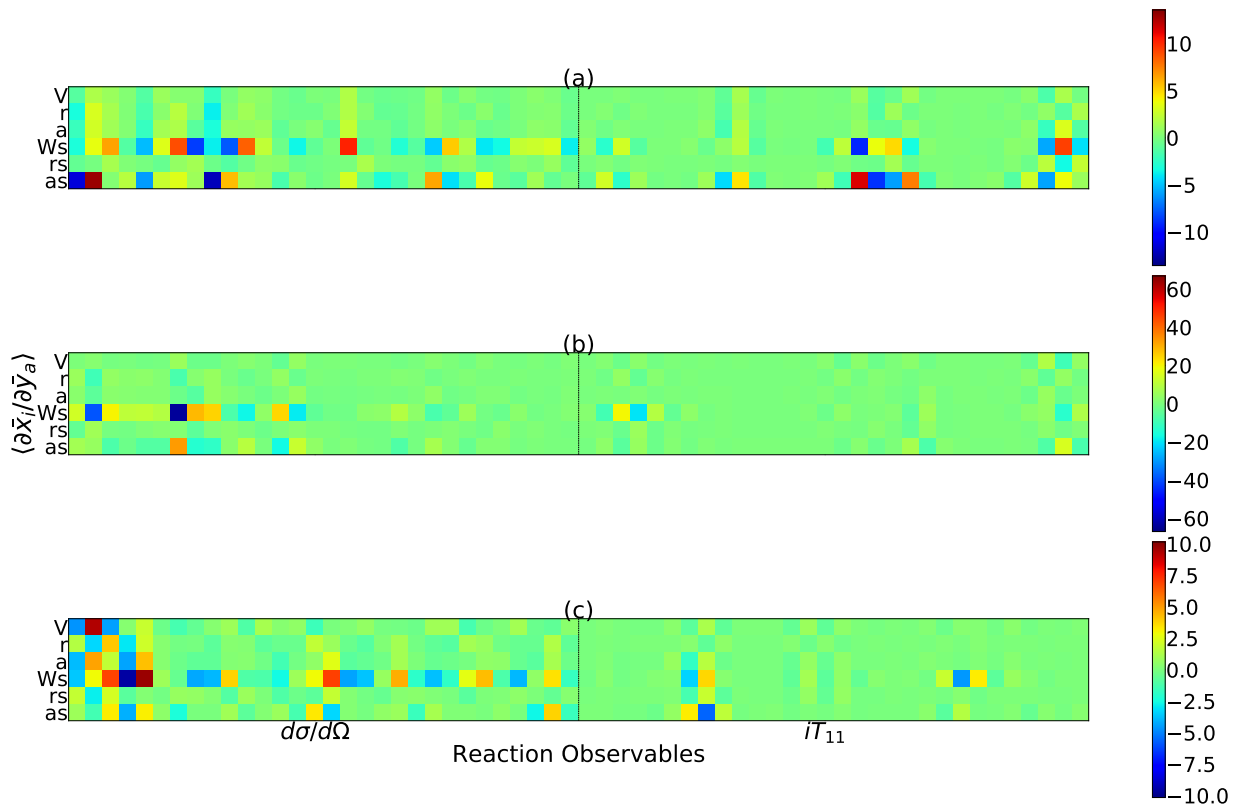


FIG. 4: Sensitivity matrix for  $\frac{d\sigma}{d\Omega}$  data and  $iT_{11}$  data: a)  $^{48}\text{Ca}(n,n)$  at 12 MeV; a)  $^{48}\text{Ca}(p,p)$  at 12 MeV and c)  $^{48}\text{Ca}(p,p)$  at 21 MeV. More details can be found in the text.

the results obtained for the sensitivities show again that the elastic angular distributions offer a better constrain on the parameters than the polarization data. Changes in the cross section angular distribution produce large changes in  $W_s$  and  $a_s$ . While some sensitivity is also seen when using polarization data, the magnitude is considerably smaller.

#### D. Principle component analysis

Given the conclusions from Section III C that these observables are mixed, the next step is to perform a principal component analysis with the intent of identifying specific combinations of observables that can be dominant in this problem. Pulling from the posterior distributions discussed in Section III B, we construct the observable covariance matrix, which is subsequently diagonalized to obtain the principle components of observable space as described in Section II. A breakdown of the contributions of the principle components to each observable considered is shown in Fig. 5. The observables indicated in the y axis are:  $\frac{d\sigma}{d\Omega}(\theta_i)$  and  $iT_{11}(\theta_i)$  for  $\theta_i = 20 - 165^\circ$  in steps of  $5^\circ$ . As can be seen, for a given observable, not all principle components are important. This suggests that, if only a given angle were of interest, one would be able

to isolate roughly a dozen terms to describe the problem.

Although the common way to analyze PCA is through the eigenvalues, it has been argued that one should instead look at the normalized weights  $w_a$  (the projection of the principle component on each observable) defined in Eq. (3). In Fig. 6, we provide the weights of the principle components for the same observables considered in Fig. 5 (panel (a) corresponds to the 12 MeV reaction while panel (b) corresponds to the 21 MeV). The strong message contained in Fig. 6 is that the weights of the principle components for the various observables are all about the same. This complicated dependence of the principal components on the original observables renders the principle component analysis less useful. Based on this analysis it would be hard to justify choosing, for instance, elastic angular distributions over polarization data.

#### E. Bayesian evidence

We now consider directly the Bayesian evidence associated with a given observable. As defined in Section II, the Bayesian evidence provides a direct measure of the information content of a given observable with regards

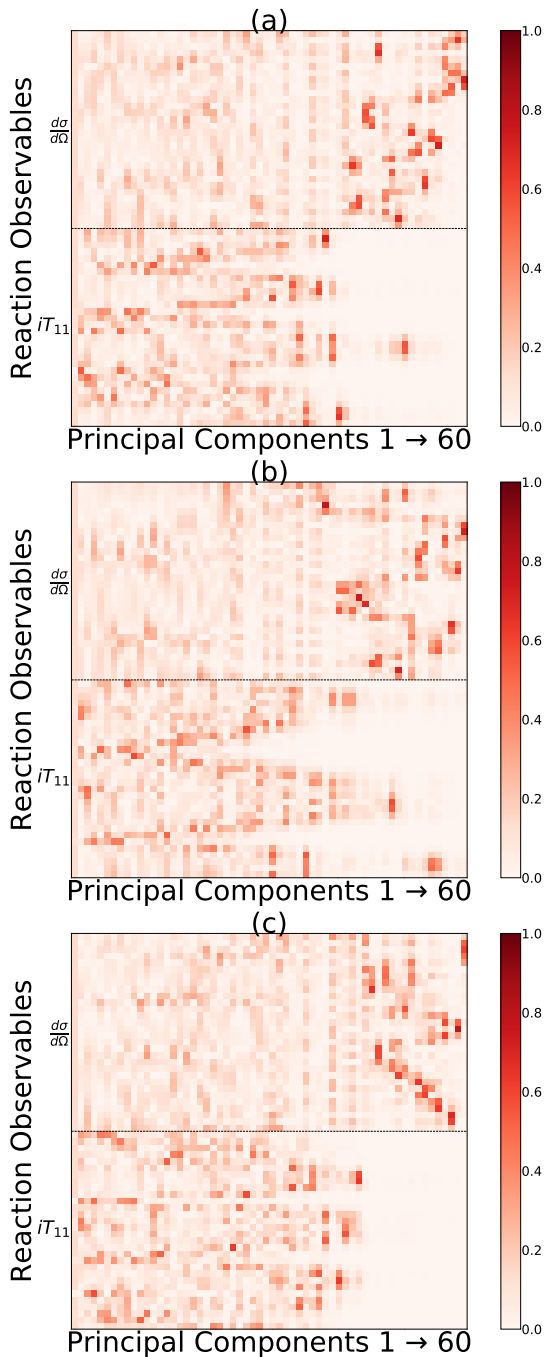


FIG. 5: Principal component analysis for  $\frac{d\sigma}{d\Omega}$  data and  $iT_{11}$  data: a)  $^{48}\text{Ca}(p,p)$  at 12 MeV and b)  $^{48}\text{Ca}(p,p)$  at 21 MeV. More details can be found in the text.

to a given model. We can then compare the values obtained when cross section angular distribution data are used and contrast these with the evidence obtained when polarization data are included instead. For obtaining the evidence, we use the same priors introduced at the top of Section III. As mentioned earlier, our problem is not amenable to an analytic treatment of the evidence inte-

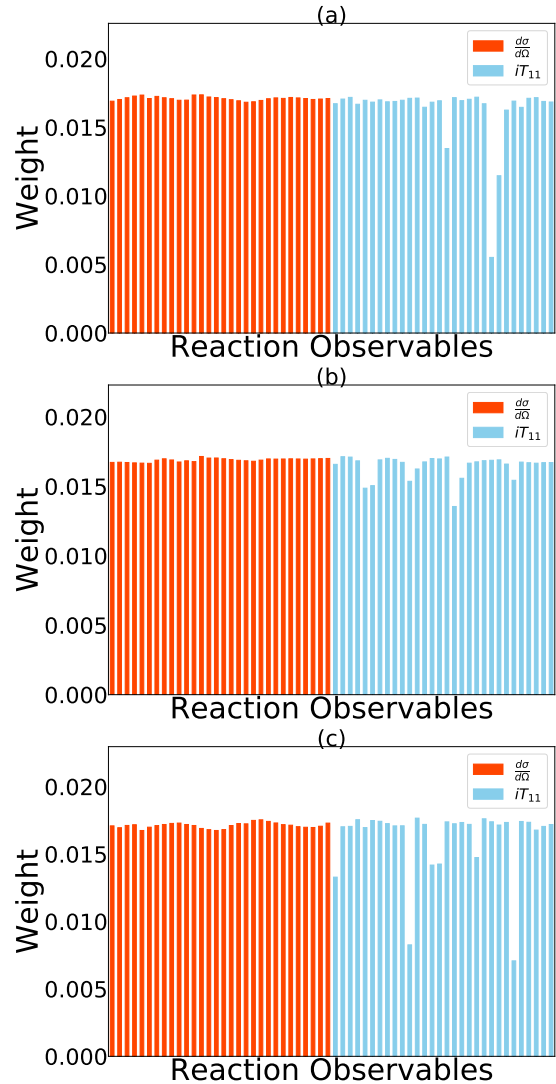


FIG. 6: Principal component weights for  $\frac{d\sigma}{d\Omega}$  data (red) or  $iT_{11}$  data (blue): a)  $^{48}\text{Ca}(p,p)$  at 12 MeV and b)  $^{48}\text{Ca}(p,p)$  at 21 MeV. More details can be found in the text.

gral thus it is very important to collect enough statistics to ensure convergence of the integral. We have studied the convergence of the evidence with the number of pulls and find that very large statistics need to be collected. Apart from small statistical fluctuations, the evidence converges when the number of parameters drawn is:  $N = 2M$  for  $^{48}\text{Ca}$  and  $N = 1.4M$  for  $^{208}\text{Pb}$ .

To minimize the effect of the statistical fluctuations, we consider an average evidence  $\bar{p}(d|\mathcal{M})$  by taking the average of the evidence at  $N = 2M, 2.2M, 2.4M$  for  $^{48}\text{Ca}$  and at  $N = 1.4M, 1.6M, 1.8M$  for  $^{208}\text{Pb}$ . The values for this average evidence are provided in Table II for all reactions considered (in parenthesis is the standard deviation). The evidence obtained for cross section data (column 2) can be easily compared by that obtained for the polarization data (column 3). The Bayes' factor, de-

fine as the ratio  $\bar{R} = \bar{p}(d|\mathcal{M})_{(d\sigma/d\Omega)}/\bar{p}(d|\mathcal{M})_{(iT_{11})}$  of the two average evidences, is shown in the last column.

The evidence for  $d\sigma/d\Omega$  data and the  $iT_{11}$  data for the reactions on  $^{48}\text{Ca}$  at 12 MeV are roughly the same, particularly taking into account the standard deviations obtained from the averaging. This is consistent with the conclusions drawn from the PCAs and the sensitivity studies. For proton scattering on  $^{48}\text{Ca}$  at the higher energy, the evidence obtained with  $d\sigma/d\Omega$  data is larger than for the  $iT_{11}$  data. This correlates with the sensitivity results shown in Fig. 4c, where larger sensitivity is found for the elastic angular distribution compared to the polarization.

A wider range of the Bayes' factor  $\bar{R}$  is obtained for the reactions on  $^{208}\text{Pb}$ . The evidence for  $d\sigma/d\Omega$  data is larger than for the  $iT_{11}$  data for neutrons on  $^{208}\text{Pb}$  at 30 MeV, while the opposite is true for the protons at the same energy. It is still unclear how to interpret these differences. We note that for example in the  $^{208}\text{Pb}(n,n)$  at 30 MeV calculations, the  $\chi^2$  (likelihood) is generally larger (smaller) for  $d\sigma/d\Omega$  than for  $iT_{11}$  (not shown), which might explain the smaller evidence obtained. For the  $^{208}\text{Pb}(p,p)$  at 30 MeV, the posteriors obtained are wider for  $d\sigma/d\Omega$  (not shown). The wider confidence intervals for  $d\sigma/d\Omega$  is accompanied with a larger evidence.

Evidently, the direct connection between sensitivity and evidence for reactions on  $^{48}\text{Ca}$  is not seen for the reactions on  $^{208}\text{Pb}$ . This highlights the fact that  $\frac{\partial \bar{x}_i}{\partial y_a}$  is essentially a very different measure than the evidence. The sensitivities in this work were obtained from averages over the posterior distributions and therefore show the rate of change in the region of parameter space defined by the posterior distributions. The evidence is an integral over the full parameter space, weighted by the likelihood. Longer tails in the likelihood result in larger evidence. Larger information content as measured in the model evidence, does not translate to tighter constraints on the parameters themselves.

Reaction	$\bar{p}(d \mathcal{M})_{(d\sigma/d\Omega)}$	$\bar{p}(d \mathcal{M})_{(iT_{11})}$	$\bar{R}$
$^{48}\text{Ca}(n,n)$ at 12 MeV	0.198(0.017)	0.190(0.044)	1.04
$^{48}\text{Ca}(p,p)$ at 12 MeV	0.142(0.043)	0.112(0.035)	1.27
$^{48}\text{Ca}(p,p)$ at 21 MeV	0.171(0.036)	0.118(0.027)	1.44
$^{208}\text{Pb}(n,n)$ at 30 MeV	0.016(0.003)	0.039(0.010)	0.42
$^{208}\text{Pb}(p,p)$ at 30 MeV	0.233(0.044)	0.086(0.018)	2.72
$^{208}\text{Pb}(p,p)$ at 61 MeV	0.157(0.051)	0.196(0.049)	0.80

TABLE II: Bayesian evidence (multiplied by  $10^{-3}$ ) for the different reactions considered: using only cross section data (2nd column), using only polarization data (3rd column), and the ratio between the Bayesian evidence with cross section data over that with polarization data (the Bayes' factor).

## IV. CONCLUSIONS

In this work we have explored a variety of diagnostic tools that allow us to go beyond uncertainty quantification toward understanding sensitivities of the parameters on the observables and the information content of a given observable. Ultimately, this provides the ability to discern between observables and thus helps optimize experiments. In particular we would like to answer the title question: Which observable offers better constraints on the optical potential?

In this work, we use the optical model and apply it to a number of reactions:  $^{48}\text{Ca}(n,n)$  at 12 MeV;  $^{48}\text{Ca}(p,p)$  at 12 MeV and 21 MeV;  $^{208}\text{Pb}(n,n)$  at 30 MeV;  $^{208}\text{Pb}(p,p)$  at 30 MeV and 61 MeV. We compare the information content of cross section angular distribution data with polarization data using a variety of statistical tools. We begin by performing standard MCMC calculations to obtain the Bayesian confidence intervals and parameter posteriors when either the elastic-scattering angular distributions is used or the vector analyzing power is used as a constraint in the optimization. We allow six parameters of the optical potential to vary, namely those associated with the real volume term and the imaginary surface term.

From the confidence intervals and the posteriors, it was difficult to determine which observable is best to constrain the optical model parameters. We then considered the sensitivity matrix constructed from the MCMC posterior distributions. This quantity describes how changes in an observable can impact the parameters under consideration. We find that, for the parameters included here, the elastic-scattering angular distributions have a larger impact on the parameter space. We also found that while for the lower energies here considered the sensitivity is primarily on the parameters of the imaginary surface term, for the higher energy the sensitivity may include the parameters of the real volume term.

Next, we performed a principal component analysis. While for a given angle, one can select a dozen of angles that are most important, overall this tool does not allow to distinguish between which of the two, angular distributions or vector analyzing powers, is best to constrain the parameters of the optical potential included in the present study.

Finally, we also computed the Bayesian evidence for each reaction. The integral over the parameter space has to be performed fully numerically, as the assumptions of Gaussian distributions for the analytic approximations were not valid. We found that in order to get converged values for the evidence, a much larger number of draws was necessary as compared to the statistics collected for the posteriors and confidence intervals. We compared the values of the evidence obtained when the cross section angular distribution was used as a constraint with those when using the polarization data. The Bayes' factor (the ratio of the two evidences) is strongly case dependent. For most cases it appears both elastic-scattering angular

distributions and polarization data have similar information content, although neutron and proton scattering on  $^{208}\text{Pb}$  show larger variability.

We note that larger information content of an observable does not imply a tighter constraint on the parameters. Our results here show that, for that purpose, the sensitivity matrix of parameters on observables is a better tool.

Further work is needed to explore the features of the Bayesian evidence in the optical model context and in particular to understand the implications of a data set having larger information content. One essential ingredient to speed up computations is to implement emulators (e.g. [24]) for optimizing the evaluation of the evidence integral. In addition, the data we included ( $d\sigma/d\Omega$  and  $iT_{11}$ ) might not give independent constraints on the optical potential because they are both associated with the same elastic scattering channel. Future plans include the

application of these tools to situations where we scrutinize between data that are more dissimilar, such as elastic scattering and charge-exchange or breakup.

### Acknowledgments

The authors would like to thank S. Pratt and M. Hirn for useful discussions on the sensitivity analysis and PCA, and L. Neufcourt for discussions on the Bayesian evidence. This work was supported by the National Science Foundation under Grant PHY-1811815 and was performed under the auspice of the U.S. Department of Energy by Los Alamos National Laboratory under Contract 89233218CNA000001. This work relied on iCER and the High Performance Computing Center at Michigan State University for computational resources.

- 
- [1] A. B. Balantekin, J. Carlson, D. J. Dean, G. M. Fuller, R. J. Furnstahl, M. Hjorth-Jensen, R. V. F. Janssens, B.-A. Li, W. Nazarewicz, F. M. Nunes, et al., *Mod. Phys. Lett. A* **29**, 31430010 (2014).
- [2] J. Rotureau, P. Danielewicz, G. Hagen, F. M. Nunes, and T. Papenbrock, *Phys. Rev. C* **95**, 024315 (2017), URL <https://link.aps.org/doi/10.1103/PhysRevC.95.024315>.
- [3] J. Rotureau, P. Danielewicz, G. Hagen, G. R. Jansen, and F. M. Nunes, *Phys. Rev. C* **98**, 044625 (2018), URL <https://link.aps.org/doi/10.1103/PhysRevC.98.044625>.
- [4] M. Burrows, C. Elster, G. Popa, K. D. Launey, A. Nogga, and P. Maris, *Phys. Rev. C* **97**, 024325 (2018), URL <https://link.aps.org/doi/10.1103/PhysRevC.97.024325>.
- [5] T. R. Whitehead, Y. Lim, and J. W. Holt, *Phys. Rev. C* **100**, 014601 (2019), URL <https://link.aps.org/doi/10.1103/PhysRevC.100.014601>.
- [6] J. Becchetti, F.D. and G. Greenlees, *Phys. Rev.* **182**, 1190 (1969).
- [7] R. Varner, W. Thompson, T. McAbee, E. Ludwig, and T. Clegg, *Physics Reports* **201**, 57 (1991), ISSN 0370-1573, URL <http://www.sciencedirect.com/science/article/pii/0370157391900390>.
- [8] A. Koning and J. Delaroche, *Nucl.Phys.* **A713**, 231 (2003).
- [9] A. E. Lovell and F. M. Nunes, *Phys. Rev. C* **97**, 064612 (2018), URL <https://link.aps.org/doi/10.1103/PhysRevC.97.064612>.
- [10] G. B. King, A. E. Lovell, L. Neufcourt, and F. M. Nunes, *Phys. Rev. Lett.* **122**, 232502 (2019), URL <https://link.aps.org/doi/10.1103/PhysRevLett.122.232502>.
- [11] M. Catacora-Rios, G. B. King, A. E. Lovell, and F. M. Nunes, *Phys. Rev. C* **100**, 064615 (2019), URL <https://link.aps.org/doi/10.1103/PhysRevC.100.064615>.
- [12] J. M. R. Fox, C. W. Johnson, and R. N. Perez, *Phys. Rev. C* **101**, 054308 (2020), URL <https://link.aps.org/doi/10.1103/PhysRevC.101.054308>.
- [13] A. Ekström and G. Hagen, *Phys. Rev. Lett.* **123**, 252501 (2019), URL <https://link.aps.org/doi/10.1103/PhysRevLett.123.252501>.
- [14] V. Kejzlar, L. Neufcourt, W. Nazarewicz, and P.-G. Reinhard, *Journal of Physics G: Nuclear and Particle Physics* (2020), URL <http://iopscience.iop.org/10.1088/1361-6471/ab907c>.
- [15] J. Novak, K. Novak, S. Pratt, J. Vredevoogd, C. E. Coleman-Smith, and R. L. Wolpert, *Phys. Rev. C* **89**, 034917 (2014), URL <https://link.aps.org/doi/10.1103/PhysRevC.89.034917>.
- [16] E. Sangaline and S. Pratt, *Phys. Rev. C* **93**, 024908 (2016), URL <https://link.aps.org/doi/10.1103/PhysRevC.93.024908>.
- [17] F. A. Gómez, C. E. Coleman-Smith, B. W. O'Shea, J. Tumlinson, and R. L. Wolpert, *The Astrophysical Journal* **760**, 112 (2012), URL <https://doi.org/10.1088%2F0004-637x%2F760%2F2%2F112>.
- [18] R. Trotta, *Contemporary Physics* **49**, 71 (2008), <http://dx.doi.org/10.1080/00107510802066753>, URL <http://dx.doi.org/10.1080/00107510802066753>.
- [19] S. Wesolowski, N. Klco, R. J. Furnstahl, D. R. Phillips, and A. Thapaliya, *Journal of Physics G: Nuclear and Particle Physics* **43**, 074001 (2016), URL <https://doi.org/10.1088%2F0954-3899%2F43%2F7%2F074001>.
- [20] V. Kejzlar, L. Neufcourt, T. Maiti, and F. Viens, *Bayesian averaging of computer models with domain discrepancies: a nuclear physics perspective* (2019), 1904.04793.
- [21] A. E. Lovell, QUILT-R: Code on Quantification of Uncertainty in Low-energy Theory for Reactions (2017).
- [22] A. E. Lovell, F. M. Nunes, J. Sarich, and S. M. Wild, *Phys. Rev. C* **95**, 024611 (2017), URL <https://link.aps.org/doi/10.1103/PhysRevC.95.024611>.
- [23] I. J. Thompson and F. M. Nunes, *Nuclear Reactions for Astrophysics* (Cambridge University Press, 2009).
- [24] R. Furnstahl, A. Garcia, P. Millican, and X. Zhang, *Physics Letters B* **809**, 135719 (2020), ISSN 0370-2693, URL <http://www.sciencedirect.com/science/article/pii/S0370269320305220>.